Journal of the European Ceramic Society 16 (1996) 843–849

S0955-2219(96)00001-5
0955-2219/96/$15.00 + .00

# Sintering and Microstructural Investigations on Combustion Processed Mullite

R. Gopi Chandran,[a] B. K. Chandrashekar,[b] C. Ganguly[c] & K. C. Patil[a*]

[a]Department of Inorganic and Physical Chemistry, Indian Institute of Science, Bangalore-560 012, India
[b]Ceramic Technological Institute, Bharat Heavy Electricals Ltd, Bangalore-560 012, India
[c]Radiometallurgy Division, Bhabha Atomic Research Centre, Bombay-400 058, India

(Received 20 September 1994; revised version received 30 November 1995; accepted 5 December 1995)

***Abstract***

*Various grades of mullite have been prepared by the combustion route using different fuels and silica sources of the redox mixture. Sintering behaviour and microstructure of combustion processed mullite have been investigated. Pure mullite sintered at 1650°C showed 3% shrinkage and was porous. The microstructure shows the presence of equiaxed grains. Hot isostatic pressing (100 MPa, 1500°C, 30 min) followed by sintering at 1700°C yielded >95% theoretical density. Mullite with 5 wt% of $Y_2O_3$ or MgO sintered at 1650°C achieved high density (≈95% theoretical density) with a shrinkage of 18 and 22% respectively. The microstructure showed the presence of anisotropic elongated mullite grains and corundum particles. The enhanced densification of mullite with additives is attributed to the formation of liquid phase which facilitates diffusion.*

## 1 Introduction

Highly pure mullite, containing less than 0·1 wt% of alkali and alkaline-earth oxides, is expected to be a superior high-temperature structural material, since its bending strength and creep resistance do not degrade even at 1200°C or more.[1,2] Similar to other crystalline ceramics with a high degree of covalent bonding, mullite also requires high temperatures for densification. This is due to its relatively low bulk and grain boundary diffusion coefficients.[3] Several processes used for the synthesis of mullite have been reviewed.[3] Recently we reported[4,5] the preparation of mullite by the combustion process using aluminium nitrate, silica fume and urea/diformyl hydrazine mixtures. At present, we report on the sintering behaviour of mullite powders obtained by the combustion of different redox mixtures, e.g. aluminium nitrate, fumed silica/fused silica/TEOS and urea/diformyl hydrazine ($C_2H_4N_2O_2$, DFH)/ carbohydrazide ($CH_6N_4O$, CH) as well as by the incorporation of extra amount of redox mixture ($NH_4NO_3/NH_4ClO_4$ and urea).

## 2 Experimental

Mullite has been prepared by the combustion of aluminium nitrate (98·5%, Glaxo, India), silica fume (99·9%, Chemicals and Plastics, India, surface area ≈200 $m^2/g$) and urea/DFH fuel according to the procedure described earlier.[4,5] DFH and CH were prepared according to the procedure described in the literature.[6,7] Mullite was prepared by the combustion of stoichiometric amounts of redox mixtures at 500°C. Details of stoichiometry calculation and combustion are given elsewhere.[4]

Various grades of mullite (M1–M7) were obtained by using different fuels, source of silica and addition of extra amount of redox mixture, e.g.:

- M1 — aluminium nitrate (20 g), silica fume (1·066 g) and urea (8 g);
- M2 — aluminium nitrate (10 g), silica fume (0·533 g), ammonium perchlorate (5 g), and urea (6·1 g);
- M3 — aluminium nitrate (10 g), ammonium nitrate (10 g), silica fume (0·533 g) and urea (10·5 g);
- M4 — aluminium nitrate (20 g), silica fume (1·066 g) and carbohydrazide (8·8 g) ($CH_6N_4O$, CH);
- M5 — aluminium nitrate (20 g), silica fume (1·066 g) and DFH ($C_2H_4N_2O_2$) (8·8 g);
- M6 — aluminium nitrate (20 g), fused silica (1·066 g) and urea (8 g) and
- M7 — aluminium nitrate (20 g) TEOS (2·7 g) and urea (8 g).

The foamy mullite obtained by combustion of redox mixtures was crushed and ground using

* To whom correspondence should be addressed.

an electric agate pestle and mortar for 3 h and used to investigate sintering and microstructure. The mullite powders were uniaxially pressed (50 MPa) to compacts of 13 mm diameter and 3–5 mm thickness, and used for sintering studies. Mullite powder derived by the urea process was milled in a pulverizer using alumina balls (3 h) to study the sintering characteristics in comparison with the unmilled powder. Particle size analysis was done on a Seishin Micron Photosizer model SKC 2000 which operates on the light scattering principle employing sedimentation. Surface area measurements were made by nitrogen adsorption employing a Micromeritics AccuSorb 2100E instrument. The temperature of the incandescent flame which appears during combustion was measured using an optical pyrometer model-120, Toshniwal Company, India. Bulk densities of the sintered compacts were measured by the Archimedes principle using distilled water. The percentage theoretical densities of sintered pellets were calculated assuming the theoretical density of mullite as 3·17 g/cm$^3$ (JCPDS 15-776). Sintering studies of mullite (M1) were carried out with different additives, e.g. $Y_2O_3$, $La_2O_3$, $CeO_2$, $TiO_2$, $ZrO_2$ and MgO. The percentage theoretical density was determined using the density of mullite and additives given in the powder diffraction file.[8] Dilatometric studies were carried out on M1 powder compacted (50 MPa) to a pellet of 11 mm diameter and 4–5 mm thickness using a Netzsch 402 E/7 dilatometer in the temperature range 20–1650°C at a heating rate of 10°/min in $N_2$ atmosphere. Dynamic shrinkage studies were also carried out on mechanically mixed 5 wt% $Y_2O_3$ and MgO-M1 powders. Microstructures of the sintered samples were observed using S-360 Cambridge scanning electron microscope (SEM) and chemical composition was determined by an energy dispersive X-ray (EDX) detector attached to the SEM. The morphology of calcined mullite (M1) powders was studied using a Philips EM 301 transmission electron microscope (TEM) operating at 100 kV.

## 3 Results and Discussion

Various phases present in the combustion derived M1–M7 were identified by the XRD and are summarized in Table 1 along with their densities and particle sizes. The M1, M4 and M5 mullites were essentially weakly crystalline with a broad peak at ≈26° (2$\theta$) in the powder XRD pattern. Complete mullitization occurred at ≈1300°C.[4,5] Mullites M2 and M3 (as-formed) prepared using extra amount of redox mixture ($NH_4NO_3/NH_4ClO_4$ and urea) were fully crystalline.[4] Changing the source of silicon to fused silica (particle size ≈10 $\mu$m) or TEOS in the combustion mixture showed the presence of $\alpha$-$Al_2O_3$ and amorphous silica. This could be due to the poor reactivity of fused silica and TEOS. Formation of mullite appears to be facilitated by silica fume due to its greater reactivity coupled with colloid formation. Thus, silica fume appears to be the ideal source of Si for the combustion synthesis of mullite (M1–M3). Further, formation of stoichiometric mullite (3:2) was confirmed by preparing various aluminosilicate powders $xAl_2O_3{\cdot}2SiO_2$, where $x$ = 1–4, by the combustion of aluminium nitrate, silica fume and urea using different mole ratios of Al:Si. The different crystalline phases formed after calcination (1400°C) are shown in Table 2. Stoichiometric mullite ($x$ = 3) gave XRD pattern of pure mullite while the one with excess alumina ($x$ = 4) and

**Table 1.** The crystalline products of combustion and bulk density*

| *Mullite* | *Phases* | *50% average size (μm)* | *Bulk density (% theoretical)* |
|---|---|---|---|
| M1 | Mullite,# $\theta$-$Al_2O_3$ | | |
| Unmilled | | 8·0 | 51 |
| Milled | | 4·0 | 61 |
| M2 | Mullite | 2·4 | 55 |
| M3 | Mullite | 4·5 | 55 |
| M4 | Mullite# | 4·2 | 61 |
| M5 | Mullite# | 3·9 | 57 |
| M6 | $\alpha$-$Al_2O_3$ | 5·8 | 51 |
| M7 | Mullite,s $\alpha$-$Al_2O_3$ | 6·3 | 56 |

*Sintered at 1600°C, # weakly crystalline, s. small amount.

**Table 2.** Surface area and phases of aluminosilicate $xAl_2O_3{\cdot}2SiO_2$ ($x$ = 1–4) powders calcined at 1400 °C, 2 h

| *Aluminosilicate* | *Surface area $m^2\,g^{-1}$ (as-formed powders)* | *Phases* |
|---|---|---|
| $1Al_2O_3{\cdot}2SiO_2$ | 201 | Mullite<br>Cristobalite<br>Corundum |
| $2Al_2O_3{\cdot}2SiO_2$ | 55 | Mullite<br>Cristobalite |
| $3Al_2O_3{\cdot}2SiO_2$(M1) | 45 | Mullite |
| $4Al_2O_3{\cdot}2SiO_2$ | 20 | Mullite<br>Corundum |

silica ($x$=1) showed the presence of corundum and cristobalite respectively besides mullite as expected.

The specific surface areas of as-prepared aluminosilicate powders vary from 20 $m^2/g$ to 200 $m^2/g$ (Table 2). The surface area of as-prepared stoichiometric mullite is 45 $m^2/g$ which increased to 200 $m^2/g$ for $1Al_2O_3{\cdot}2SiO_2$. This increase in surface area could be attributed to the amorphous nature of the sample and also due to the very low flame temperature (900°C) compared to the $4Al_2O_3{\cdot}2SiO_2$ (temperature ≈1400°C), which had the lowest surface area, 20 $m^2/g$. Thus, the surface area of aluminosilicates ($Al_2O_3$–$SiO_2$ system) appears to be controlled by the alumina content and processing conditions.

### 3.1 Dilatometry and sintering of mullite

The dilatometric curve of M1 compact is shown in Fig. 1. The shrinkage curve shows two clearly defined zones:

(i) Negligible shrinkage took place up to 1000°C and

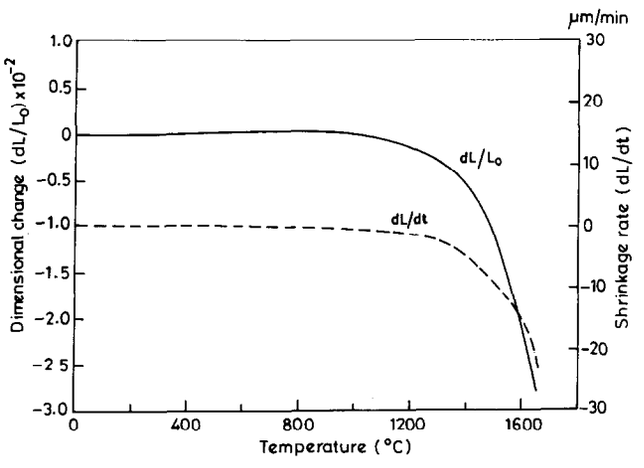


**Fig. 1.** Dynamic shrinkage curve of M1.

(ii) Between 1100 and 1650°C the total linear shrinkage was less than 3% with a shrinkage rate of ≈25 μm/min.

The green density of M1 uniaxially pressed at 50 MPa was 1·5264 $g/cm^3$ which on sintering at 1650°C (2 h) became 1·6854 $g/cm^3$. The milled powder attained a density of 1·9337 $g/cm^3$. The TEM of M1 particles is shown in Fig. 2. It could

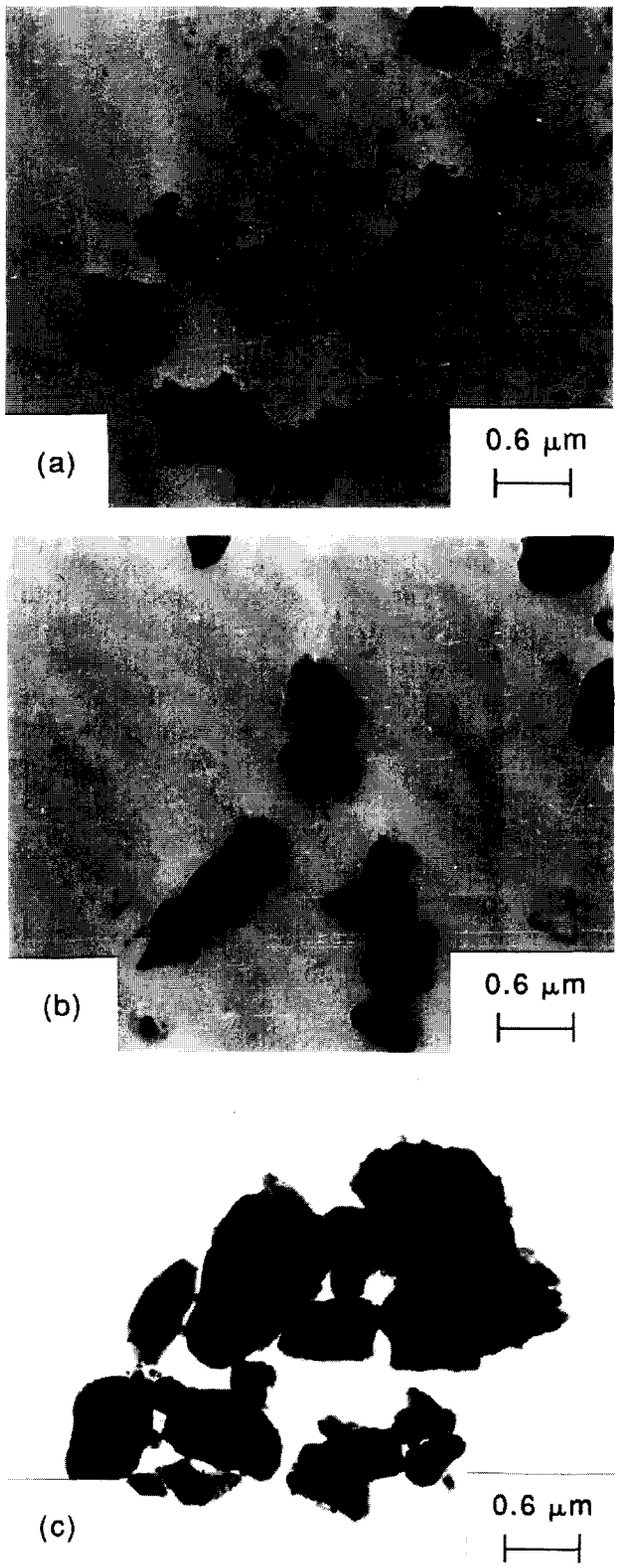


**Fig. 2.** TEM of M1(a) calcined at 1000°C; (b) calcined at 1200°C and (c) calcined at 1400°C for 1 h.

be seen that the particles have an irregular plate morphology which remains so even after calcination at 1400°C. The low density achieved on sintering could probably be due to the irregular plate morphology of the particles, lower green density and also partly due to the appearance of flame during combustion which induces mullite[9,10] crystallization and neck growth processes. It is interesting to note that combustion derived mullite appears to behave like reaction sintered mullite rather than sol–gel mullite although particle sizes are comparable to sol–gel powders. The as-formed combustion derived powders are crystalline and probably is the reason for lower density achieved as no viscous sintering was possible.

### 3.2 Effect of processing parameters on particle size and density of mullite

The particle size distributions of the mullite powders M4 and M5 are shown in Fig. 3 and compared with M1. Mullite powders prepared by CH (M4) and DFH (M5) processes have smaller particle size (4 $\mu$m). It is comparable to milled mullite M1 (Table 1). Though the powders were fine, the final density of sintered mullite was very low. Lowering the particle size results in increase of the neck growth processes leading to aggregate formation. Aggregates are known[3] to hinder sintering of the compact. In the case of samples wherein mullite crystallites are nucleated, higher density could be attained usually by long milling times[3,9] or hot pressing techniques.[10] Milling appears to help in the breaking of the aggregates ($\geq$0·5 $\mu$m) but introduces contamination from the grinding media. Sintered densities of mullite compacts prepared from different size mullites are listed in Table 1. It could be seen that the sintered mullite compacts are porous (Table 1). In addition to reducing the average particle size, sintering can also be enhanced by improving the packing characteristics of the green compact, i.e. increasing green density, decreasing the average pore size and eliminating large defects. Uniaxially pressed samples tend to have relatively large inhomogeneities as a result of the initial packing irregularities created during die filling and the non-uniform stress gradients generated during compaction.[3]

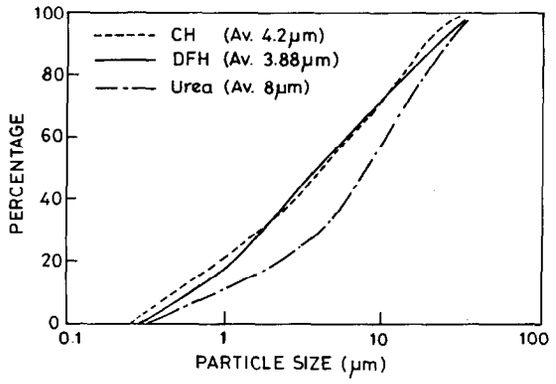


**Fig. 3.** Particle size distributions (cumulative weight percentage) of mullite prepared using urea (M1), CH (M4) and DFH (M5) processes.

Mullite (M1) when pressed uniaxially and sintered at 1600°C, 2 h achieved a density of 51% theoretical while when pressed cold isostatically (210 MPa) and sintered at 1600°C achieved a density of 63%. Higher density (>95%) could be achieved by hot isostatic pressing (100 MPa, 1500°C, 30 min) followed by sintering at 1700°C, 30 min. The microstructure of the isostatically pressed and sintered M1 (Fig. 4) shows the porous nature of the sample as expected from the density measurements. The microstructure consisted of large agglomerates interconnected by pores (Fig. 4(a)); each aggregate, however, was fully dense and was composed of submicrometer equiaxed grains (Fig. 4(b)). It is generally believed that the presence of a liquid phase causes anisotropic grains. It is known[11] that a metastable $SiO_2$-rich liquid phase can exist even at temperatures as low as 1250°C in the case of diphasic gels. Mullite processed from colloidal (diphasic) gel[12] is rich in $Al_2O_3$ resulting

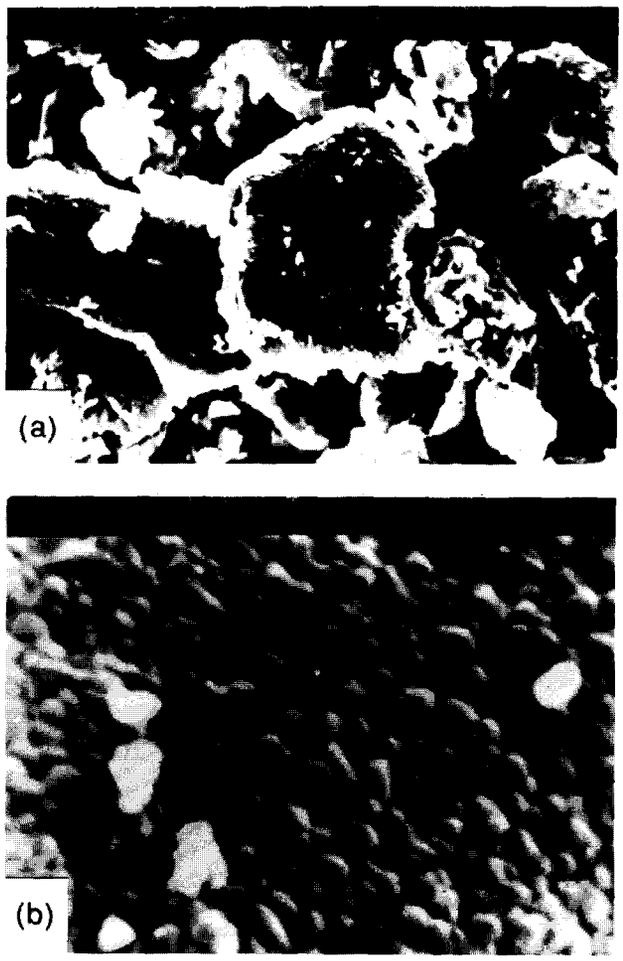


**Fig. 4.** (a) The microstructure of M1 sintered at 1600°C and (b) microstructure at higher magnification.

**Table 3.** Bulk density of mullite (M1) + additives sintered at 1650°C

| *Additive (5 wt%)* | *Bulk density (g/cm³)** |
|---|---|
| — | 1·68 (53) |
| $Y_2O_3$ | 3·12 (95·7) |
| MgO | 3·06 (95·9) |
| $TiO_2$ | 2·07 (64·3) |
| $ZrO_2$ | 1·89 (57·4) |
| $CeO_2$ | 2·89 (85·8) |
| $La_2O_3$ | 2·78 (83·2) |

*Values in the parentheses correspond to % theoretical density.

in a $SiO_2$-rich liquid phase. However, there are other reports of equiaxed grains from diphasic gels[13,14] and anisotropic grains from single phase gels.[15–17] Though combustion processed mullite starts from diphasic redox mixture, the microstructure was composed of submicrometer equiaxed grains indicating the absence of liquid phase and hence very low shrinkage during sintering (Fig. 1). Li and Thomson[17] have shown the importance of chemical composition on the morphology of mullite grains. They could make mullite with anisotropic and equiaxed grains from both single phase and diphasic gels by controlling the $Al_2O_3/SiO_2$ ratio near the stoichiometric mullite.

### 3.3 Effect of additives on sintering

Additives (0–5 wt%) like MgO, $ZrO_2$, $TiO_2$, and rare earth oxides like $Y_2O_3$, $La_2O_3$ and $CeO_2$ have been used to study their effect on the sintering behavior of mullite (M1). The densities of mullite with 5 wt% additives sintered at 1650°C are summarized in Table 1. The final density at 1650°C, 2 h was very low for 5 wt% of $TiO_2$, $ZrO_2$ and $La_2O_3$ and ranges from 1·9 to 2·9 g/cm³. Addition of 5 wt% of $CeO_2$, however gave a density of 2·89 g/cm³ and its microstructure showed acicular grains. 5 wt% of magnesia and yttria additives gave a highest density of 3·06 and 3·12 g/cm³ respectively and the sintering behaviour of these was studied.

### 3.4 Dilatometric studies of mullite-MgO/$Y_2O_3$ (5 wt%)

Dynamic sintering studies of mullite-magnesia (5 wt%) and mullite-yttria (5 wt%) were performed on compacts in the temperature range 25–1650°C. The powders were uniaxially pressed at 50 MPa (without deagglomeration of the platelets) and the shrinkage versus temperature was measured at a constant heating rate of 10°/min. The dilatometric curves of mullite-magnesia (5 wt%)

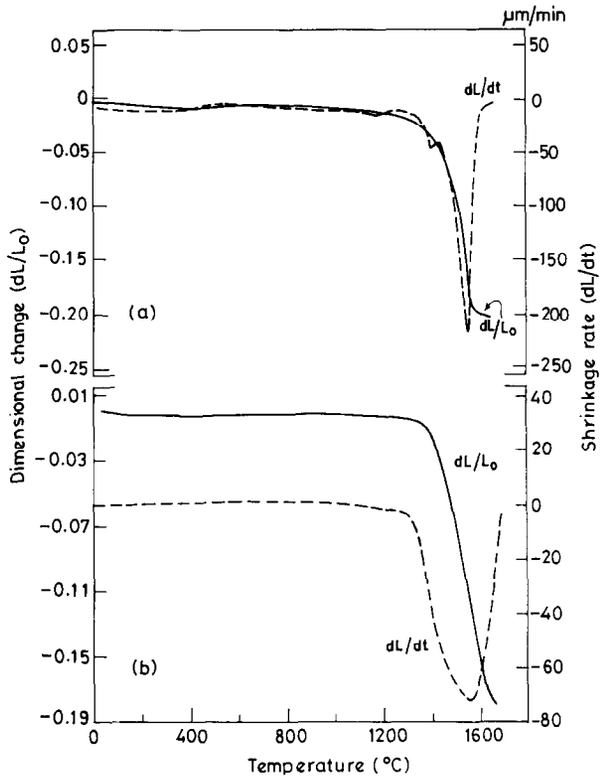


**Fig. 5.** Dilatometric curves of (a) mullite (M1)-magnesia (5 wt%) and (b) mullite (M1)-yttria (5 wt%).

and mullite-yttria (5 wt%) are given in Fig. 5. Both magnesia- (Fig. 5(a)) and yttria-mullite (Fig. 5(b)) show single step shrinkage. No shrinkage was seen until 1400°C in both the cases, after which a sharp shrinkage was noticed, total shrinkage being 22 and 18% respectively. The shrinkage rate of magnesia- and yttria-mullite was 220 and 75 μm/min respectively at 1650°C. Unlike gel-derived mullite,[18–20] which shows sharp shrinkage before mullitization, combustion derived powders show shrinkage after mullitization. This could be attributed to the formation of liquid phase which helps in the rearrangement of the particles followed by densification. In the gel-derived samples the initial shrinkage before mullite nucleation is attributed to the viscous flow which stops once mullite is nucleated.[18,19]

The dependence of density on the percentage of magnesia and yttria additives at sintering temperature of 1575°C, 2 h is shown in Fig. 6. A steady increase in the density was observed with the increase in percentage of the additives. The variation of density with temperature for 5 wt% of MgO and $Y_2O_3$-mullite is shown in Fig. 7. It could be seen that the density increases beyond 1400°C as expected from the dilatometric studies (Fig. 5). The final density was above 3·0 g/cm³ at 1650°C. The microstructures of (5 wt%) MgO and $Y_2O_3$ mullite sintered at 1600°C are shown in Figs 8 and 9 respectively. The mullite with MgO additive

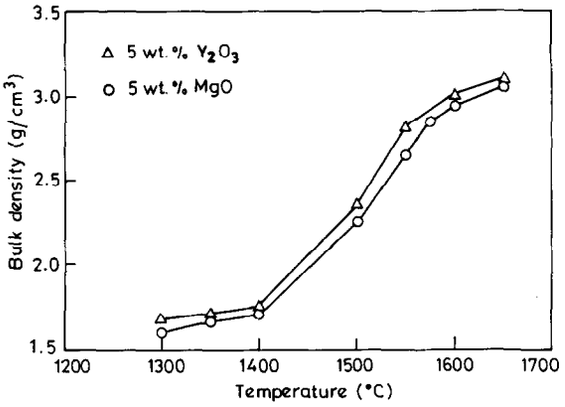


**Fig. 6.** Dependence of density of mullite on the percentage of magnesia and yttria (1–5 wt%) at 1575°C, 2 h.

show a very dense microstructure with acicular grains, the chemical composition of the grain correspond to that of mullite. Similar observation was made in the case of yttria-mullite (Fig. 9). The microstructures of 5 wt% MgO and $Y_2O_3$-mullite sintered at 1600°C show the presence of corundum in certain regions of the compact. A typical

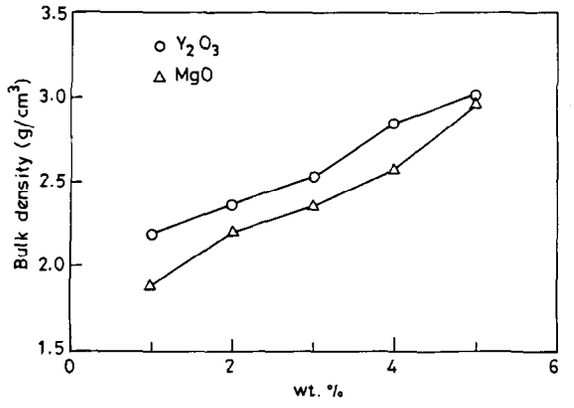


**Fig. 7.** Variation of density of mullite (M1)-magnesia/yttria (5 wt%) as a function of sintering temperature.


**Fig. 8.** Microstructure of mullite (M1)-magnesia (5 wt%) sintered at 1600°C, 2 h.


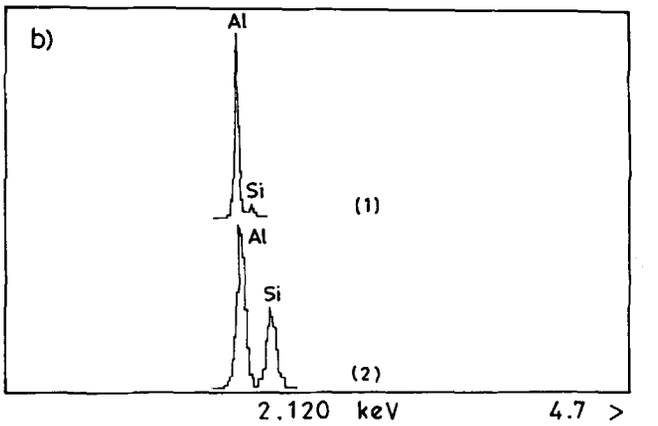


**Fig. 9.** (a) Microstructure of mullite (M1)-yttria (5 wt%) sintered at 1600°C, 2 h and (b) EDX of the grain marked 1 and 2 in (b).

microstructure of yttria-mullite showing corundum and mullite grains is shown in Fig. 9. It is interesting to note that while the microstructure of pure sintered mullite was composed of submicrometer equiaxed grains (Fig. 4(b)), the one with additives was elongated with large increase in the grain size (Figs 8 and 9). The large increase in the size of mullite grains is probably due to the formation of liquid phase which allow rapid transport of material and much more rapid grain growth similar to the one observed in the case of sodium-doped mullite.[21]

Addition of $Y_2O_3$ or MgO in the $Al_2O_3$–$SiO_2$ system forms a liquid phase at low temperatures and promotes the densification.[22,23] It is interesting to note that densities greater than 3·0 g/cm$^3$ could be achieved at 1650°C, but the density of mullite without the additive was less than 2·0 g/cm$^3$. During sintering some crystalline phases of yttrium silicate or magnesium aluminate spinel were formed in addition to mullite and corundum by the crystallization of the liquid phases as the furnace cooled. In the case of $Y_2O_3$-mullite crystalline phases of Y-silicate and corundum were observed by Fang and Hwang.[22,23] The liquid phase formed

at higher sintering temperature enhanced the sinterability of mullite powders. During the furnace cooling process, the liquid phase crystallized (by solution–reprecipitation process) and different crystalline phases were obtained depending on the amount of $Y_2O_3$.[22,23] Yttria and magnesia appear to be the best additives for achieving high density in combustion derived mullite.

## 4 Conclusions

(i) Pure mullite prepared by the combustion process when sintered at high temperatures (1600°C) was porous and composed of equiaxed grains.
(ii) Mullite could be sintered to high density (95% theoretical) by hot isostatic pressing or by the use of liquid-forming additives like MgO or $Y_2O_3$.
(iii) Dynamic shrinkage studies of mullite with additives showed the shrinkage to take place after 1400°C, with a total shrinkage of 18 and 22% for yttria and magnesia, respectively.
(iii) The microstructures of magnesia- and yttria-mullite show the presence of anisotropic grains of mullite and alumina particles.

## Acknowledgements

The authors thank Mr L. N. Satpathy, BHEL, for his help. One of the authors (RGC) is grateful to the Council of Scientific and Industrial Research (CSIR), New Delhi, India for the award of a Senior Research fellowship.

## References

1. Kanzaki, S., Tabata H., Kumazawa, T. & Ohta S., Sintering and Mechanical Properties of Stoichiometric Mullite. *J. Am. Ceram. Soc.*, **68** (1985) C6–C7.
2 Dokko. P. C., Pask, J. A. & Mazdiyasni, K. S., High-Temperature Mechanical Properties of Mullite Under Compression. *J. Am. Ceram. Soc.*, **60** (1977) 150–5.
3. Sacks, M. D., Lee. H. W. & Pask, J. A., A Review of Powder Preparation Methods and Densification Procedures For Fabricating High Density Mullite. In *Mullite and Mullite Matrix Composites, Ceramic Transactions*, Vol. 6, ed. S. Somiya, R. F. Davis & J. A. Pask. The American Ceramic Society Inc., Westerville, OH, 1990, pp. 167–207.
4. Gopi Chandran, R. & Patil, K. C., A Rapid Combustion Method for the Preparation of Crystalline Mullite Powders. *Mater. Lett.*, **10** (1990) 291–5.
5. Gopi Chandran, R., Chandrappa, G. T. & Patil, K. C., Combustion Synthesis of Oxide Materials using Metal nitrates-diformyl hydrazine Redox Mixtures, *Int. J. Self-Prop. High-Temp. Synth.*, **3** (1994) 131–42.
6. Ainsworth, C. & Jones, R. G., Isomeric and Nuclear-substituted $\beta$-Aminoethyl-1,2,4-triazoles. *J. Am. Chem. Soc.*, **77** (1955) 621–4.
7. Mohr, E. B., Brezinki, J. J. & Andrieth, L. F., Carbohydrazide. In *Inorganic Synthesis*, Vol. 4, McGraw Hill, New York, 1953, pp. 32–5.
8. Powder Diffraction File, Joint Committee on Diffraction Standards, Swarthmore, PA, 1988.
9. Metcalf, B. L. & Sant, J. H., The Synthesis, Microstructure and Physical Properties of High Purity Mullite. *Trans. J. Brit. Ceram. Soc.*, **74** (1975) 193.
10. Mazdiyasni, K. S., Preparation and characterization of mullite powders from alkoxides and other chemical routes. In *Mullite and Mullite Matrix Composites, Ceramic Transactions, Vol. 6*, The American Ceramic Society Inc., Westerville, OH, 1990, pp. 243–53.
11. Aksay, I. A. & Pask, J. A., Stable and Metastable Equilibria in the System $SiO_2$–$Al_2O_3$. *J. Am. Ceram. Soc.*, **58** (1975) 507–12.
12. Pask J. A., Zhang, Y. W., Tomsia, A. P. & Yoldas, B. E., Effect of Sol–Gel Mixing on Mullite Microstructure and Phase Equilibria in the $\alpha$-$Al_2O_3$–$SiO_2$ System. *J. Am. Ceram. Soc.*, **70** (1987) 704–7.
13. Huling, J. C. & Messing, G. L., Hybrid Gels for Homoepitactic Nucleation of Mullite. *J. Am. Ceram. Soc.*, **72** (1989) 1725–9.
14. Wei, W. C. & Halloran, J. W., Phase Transformation of Diphasic Aluminosilicate Gels. *J. Am. Ceram. Soc.*, **71** (1988) 581–7.
15. Li, D. X. & Thomson, W. J., Kinetic Mechanisms for the Mullite Formation From Sol–Gel Precursors. *J. Mater. Res.*, **57** (1990) 1963–9.
16. Mazdiyasni, K. S. & Brown, L. M., Synthesis and Mechanical Properties of Stoichiometric Aluminium Silicate (Mullite). *J. Am. Ceram. Soc.*, **55** (1972) 548–52.
17. Li, D. X. & Thomson, W. J., Mullite Formation From Nonstoichiometric Diphasic Precursors. *J. Am. Ceram. Soc.*, **74** (1991) 2382–7.
18. Osendi, M. I., Baudin, C., de Aza, S. & Moya, J. S., Processing and Sintering of 3:2 Alumina Silica Gel. *Ceram. Int.*, **18** (1992) 365–72.
19. Osendi, M. I., Baudin, C. & de Aza, S., Mullite Material from a 3:2 Alumina–Silica Gel. Part II: Microstructural Evolution. *J. Eur. Ceram. Soc.*, **10** (1992) 399–403.
20. Douy, A., Organic Gels in the Preparation of Silico-aluminate Powders. I: Mullite. *J. Eur. Ceram. Soc.*, **7** (1991) 117–23.
21. Fahrenholtz, W. G. & Smith D. M., Densification and Microstructure of Sodium-Doped Colloidal Mullite. *J. Am. Ceram. Soc.*, **17** (1994) 1377–80.
22. Fang, D. Y. & Hwang, C. S., Effects of $Y_2O_3$ addition on the Sinterability and Microstructure of Mullite: I. Phase Transformation and Sinterability. J. *Ceram. Soc. Jpn, Int. Ed.*, **100** (1992) 1141–6.
23. Fang, D. Y. & Hwang, C. S., Effects of $Y_2O_3$ addition on the Sinterability and Microstructure of Mullite: II. Crystallization of Liquid Phase and Grain Growth. *J. Ceram. Soc. Jpn, Int. Ed.*, **101** (1993) 322–6.